# 錯体化学Ⅱ 資料1

錯体物性化学　大場正昭

ohba@chem.kyushu-univ.jp
092-802-4052

*Inorganic Chemistry*: Housecroft and Sharpe 4th Ed.
*Inorganic Chemistry*: Shriver and Atkins 5th Ed.

## 分光化学系列



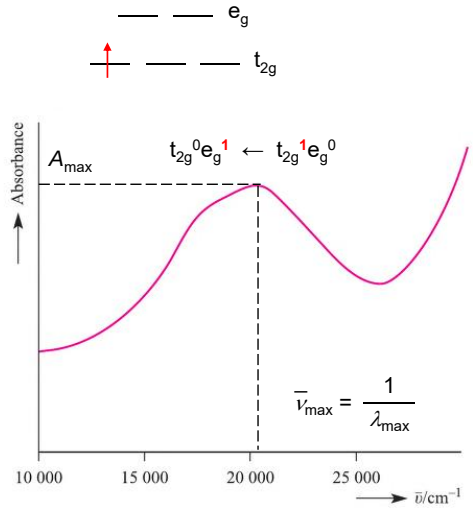


**Fig. 20.4** The electronic absorption spectrum of $[Ti(OH_2)_6]^{3+}$ in aqueous solution.

$$\varepsilon_{max} = \frac{A_{max}}{c \times \ell} \qquad (\varepsilon_{max} \text{ in dm}^3\,\text{mol}^{-1}\,\text{cm}^{-1})$$

**Table 20.2** Values of $\Delta_{oct}$ for some *d*-block metal complexes.

| Complex | $\Delta$ / cm$^{-1}$ | Complex | $\Delta$ / cm$^{-1}$ |
|---|---|---|---|
| $[TiF_6]^{3-}$ | 17 000 | $[Fe(ox)_3]^{3-}$ | 14 100 |
| $[Ti(OH_2)_6]^{3+}$ | 20 300 | $[Fe(CN)_6]^{3-}$ | 35 000 |
| $[V(OH_2)_6]^{3+}$ | 17 850 | $[Fe(CN)_6]^{4-}$ | 33 800 |
| $[V(OH_2)_6]^{2+}$ | 12 400 | $[CoF_6]^{3-}$ | 13 100 |
| $[CrF_6]^{3-}$ | 15 000 | $[Co(NH_3)_6]^{3+}$ | 22 900 |
| $[Cr(OH_2)_6]^{3+}$ | 17 400 | $[Co(NH_3)_6]^{2+}$ | 10 200 |
| $[Cr(OH_2)_6]^{2+}$ | 14 100 | $[Co(en)_3]^{3+}$ | 24 000 |
| $[Cr(NH_3)_6]^{3+}$ | 21 600 | $[Co(OH_2)_6]^{3+}$ | 18 200 |
| $[Cr(CN)_6]^{3-}$ | 26 600 | $[Co(OH_2)_6]^{2+}$ | 9 300 |
| $[MnF_6]^{2-}$ | 21 800 | $[Ni(OH_2)_6]^{2+}$ | 8 500 |
| $[Fe(OH_2)_6]^{3+}$ | 13 700 | $[Ni(NH_3)_6]^{2+}$ | 10 800 |
| $[Fe(OH_2)_6]^{2+}$ | 9 400 | $[Ni(en)_3]^{2+}$ | 11 500 |

Spectrochemical series

$I^- < Br^- < [NCS]^- < Cl^- < F^- < [OH]^- < [ox]^{2-}$
$\approx H_2O < [NCS]^- < NH_3 < en < bpy < phen < [CN]^- \approx CO$
weak field ligands → strong field
ligands increasing $\Delta_{oct}$

## Ti(III) および Cr(III) 錯体の吸収スペクトル



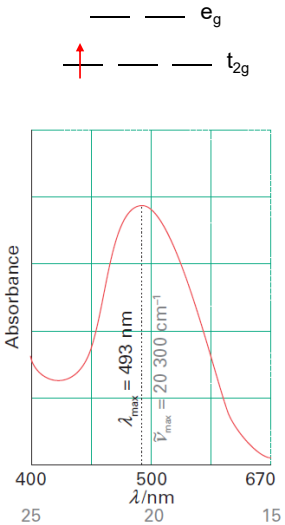


**Figure 20.3** The optical absorption spectrum of $[Ti(OH_2)_6]^{3+}$.

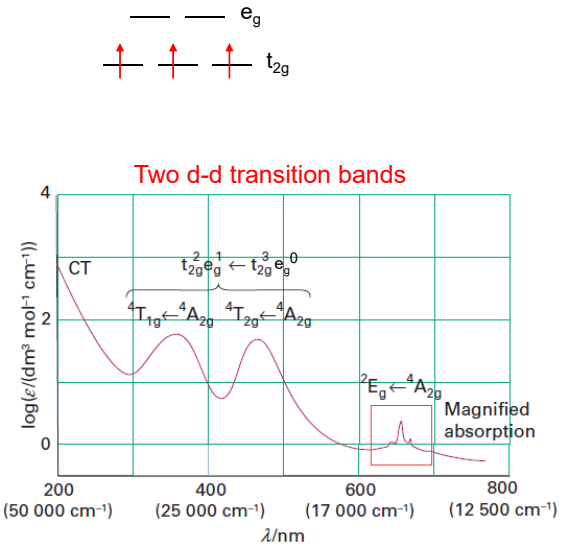


**Figure 20.22** The spectrum of the $d^3$ complex $[Cr(NH_3)_6]^{3+}$, which illustrates the features studied in this section, and the assignments of the transitions as explained in the text.

## 金属イオンおよび配位子群軌道の対称性



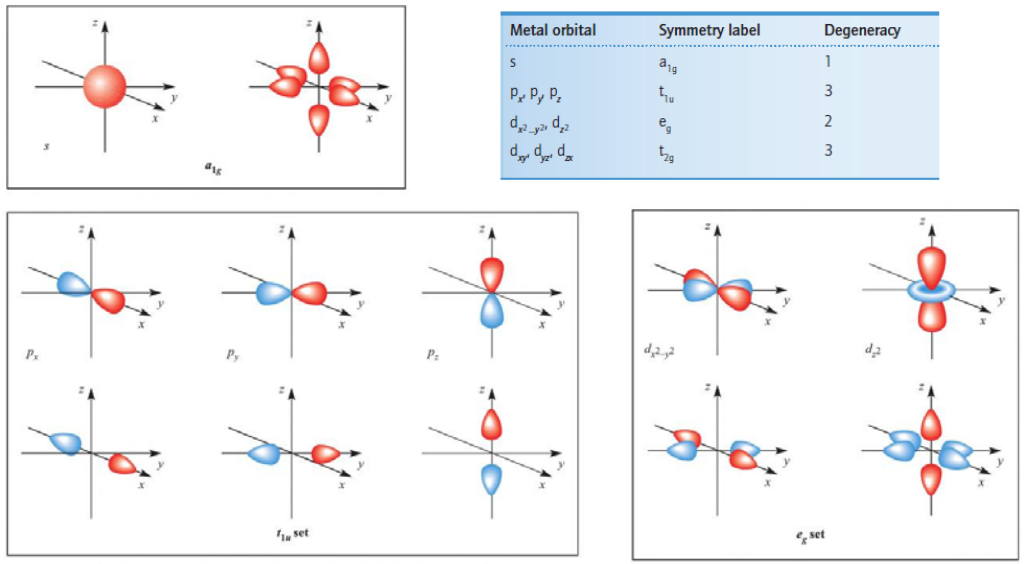


**Fig. 20.12** Metal atomic orbitals $s$, $p_x$, $p_y$, $p_z$, $d_{x^2-y^2}$, $d_{z^2}$ matched by symmetry with ligand group orbitals for an octahedral ($O_h$) complex with only $\sigma$-bonding.

## $ML_6$ ($O_h$) 錯体の分子軌道図（σ 結合のみの場合） 4

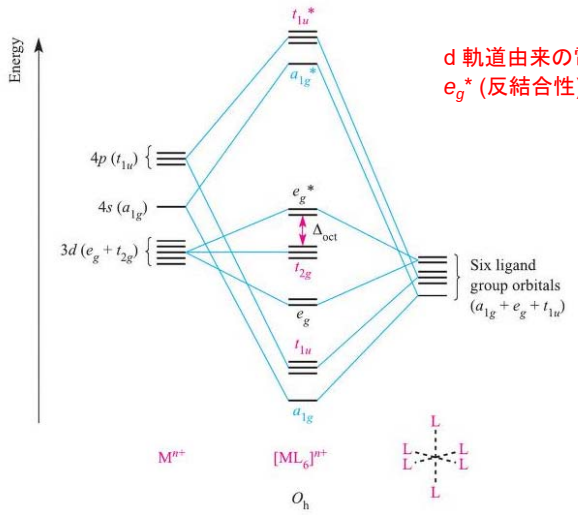


d 軌道由来の電子は、$t_{2g}$ (非結合性) と $e_g$* (反結合性) に充填

σ 供与性 (ルイス塩基性) の増大
↓
$e_g$* 軌道の不安定化
↓
$\Delta_{oct}$ の増大

**Fig. 20.13** An approximate MO diagram for the formation of $[ML_6]^{n+}$ (where M is a first row metal) using the ligand group orbital approach; the orbitals are shown pictorially in Fig. 20.12. The bonding only involves M−L σ-interactions.

## d 軌道と配位子間の π 結合の様式 5

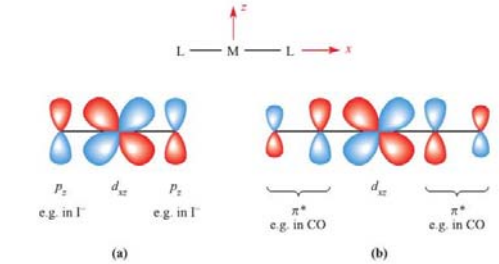


**Fig. 20.14** π-Bond formation in a linear L−M−L unit in which the metal and ligand donor atoms lie on the $x$ axis: (a) between metal $d_{xz}$ and ligand $p_z$ orbitals as for L = $I^-$, an example of a π-donor ligand, and (b) between metal $d_{xz}$ and ligand $\pi^*$-orbitals as for L = CO, an example of a π-acceptor ligand.

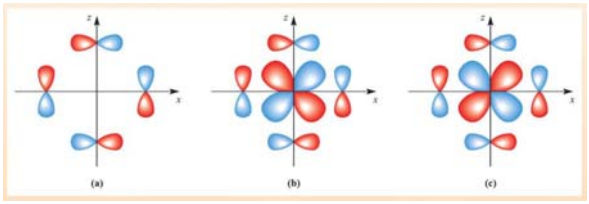


**Box 20.2 The $t_{2g}$ set of ligand π-orbitals for an octahedral complex**

## $ML_6$ ($O_h$) 錯体の分子軌道図（π 供与性配位子） 6

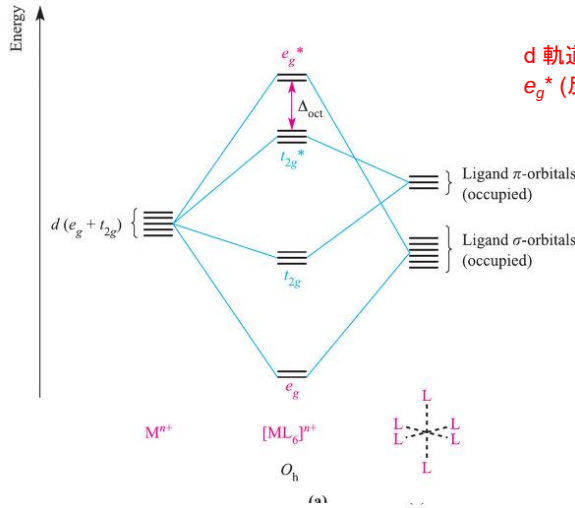


d 軌道由来の電子は、$t_{2g}$* (反結合性) と $e_g$* (反結合性) に充填

π 供与性の増大
↓
$t_{2g}$* 軌道の不安定化
↓
$\Delta_{oct}$ の減少

**Fig. 20.15** Approximate partial MO diagrams for metal–ligand π-bonding in an octahedral complex: (a) with π-donor ligands and (b) with π-acceptor ligands. In addition to the MOs shown, σ-bonding in the complex involves the $a_{1g}$ and $t_{1u}$ MOs (see Fig. 20.13). Electrons are omitted from the diagram, because we are dealing with a general $M^{n+}$ ion. Compared with Fig. 20.13, the energy scale is expanded.

## $ML_6$ ($O_h$) 錯体の分子軌道図（π 受容性配位子） 7

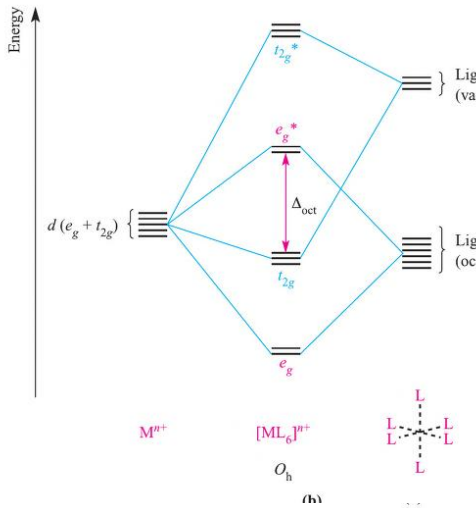


d 軌道由来の電子は、$t_{2g}$ (結合性) と $e_g$* (反結合性) に充填

π 逆供与 (back donation)
Metal-to-ligand Charge Transfer (MLCT)

π 受容性の増大
金属イオンの π 供与性の増大
↓
$t_{2g}$ 軌道の安定化
↓
$\Delta_{oct}$ の増大

**Fig. 20.15** Approximate partial MO diagrams for metal–ligand π-bonding in an octahedral complex: (a) with π-donor ligands and (b) with π-acceptor ligands. In addition to the MOs shown, σ-bonding in the complex involves the $a_{1g}$ and $t_{1u}$ MOs (see Fig. 20.13). Electrons are omitted from the diagram, because we are dealing with a general $M^{n+}$ ion. Compared with Fig. 20.13, the energy scale is expanded.

# $O_h$ および $T_d$ 点群の指標表



**The cubic groups**

| $T_d$ (43$m$) | $E$ | $8C_3$ | $3C_2$ | $6S_4$ | $6\sigma_d$ | $h = 24$ | |
|---|---|---|---|---|---|---|---|
| $A_1$ | 1 | 1 | 1 | 1 | 1 | | $x^2 + y^2 + z^2$ |
| $A_2$ | 1 | 1 | 1 | −1 | −1 | | |
| E | 2 | −1 | 2 | 0 | 0 | | $(2z^2 - x^2 - y^2, x^2 - y^2)$ |
| $T_1$ | 3 | 0 | −1 | 1 | −1 | $(R_x, R_y, R_z)$ | |
| $T_2$ | 3 | 0 | −1 | −1 | 1 | $(x, y, z)$ | $(xy, yz, zx)$ |

| $O_h$ ($m3m$) | $E$ | $8C_3$ | $6C_2$ | $6C_4$ | $3C_2(=C_4^2)$ | $i$ | $6S_4$ | $8S_6$ | $3\sigma_h$ | $6\sigma_d$ | $h = 48$ | |
|---|---|---|---|---|---|---|---|---|---|---|---|---|
| $A_{1g}$ | 1 | 1 | 1 | 1 | 1 | 1 | 1 | 1 | 1 | 1 | | $x^2 + y^2 + z^2$ |
| $A_{2g}$ | 1 | 1 | −1 | −1 | 1 | 1 | −1 | 1 | 1 | −1 | | |
| $E_g$ | 2 | −1 | 0 | 0 | 2 | 2 | 0 | −1 | 2 | 0 | | $(2z^2 - x^2 - y^2, x^2 - y^2)$ |
| $T_{1g}$ | 3 | 0 | −1 | 1 | −1 | 3 | 1 | 0 | −1 | −1 | $(R_x, R_y, R_z)$ | |
| $T_{2g}$ | 3 | 0 | 1 | −1 | −1 | 3 | −1 | 0 | −1 | 1 | | $(xy, yz, zx)$ |
| $A_{1u}$ | 1 | 1 | 1 | 1 | 1 | −1 | −1 | −1 | −1 | −1 | | |
| $A_{2u}$ | 1 | 1 | −1 | −1 | 1 | −1 | 1 | −1 | −1 | 1 | | |
| $E_u$ | 2 | −1 | 0 | 0 | 2 | −2 | 0 | 1 | −2 | 0 | | |
| $T_{1u}$ | 3 | 0 | −1 | 1 | −1 | −3 | −1 | 0 | 1 | 1 | $(x, y, z)$ | |
| $T_{2u}$ | 3 | 0 | 1 | −1 | −1 | −3 | 1 | 0 | 1 | −1 | | |